In-line acousto-optic interferometer as a correlator and spectrum analyzer

Riza, Nabeel

Nabeel A. Riza, "In-line acousto-optic interferometer as a correlator and spectrum analyzer," Proc. SPIE 2026, Photonics for Processors, Neural Networks, and Memories, (9 November 1993); doi: 10.1117/12.163566

SPIE.

Event: SPIE's 1993 International Symposium on Optics, Imaging, and Instrumentation, 1993, San Diego, CA, United States

The In-line Acousto-optic Interferometer as a Correlator and Spectrum Analyzer

Nabeel A. Riza
General Electric Corporate Research and Development Center
P. O. Box 8, KWB 617, Schenectady, N.Y. 12301

ABSTRACT

A novel, efficient, stable, in-line, two Bragg cell, acousto-optic architecture is introduced for signal correlation and spectrum analysis, and experimental results are described. The processor employs an image inversion technique to produce a correlation output that does not have to be generated on a spatial carrier. The system is particularly suited for wide instantaneous bandwidth signal processing.

2. INTRODUCTION

Correlation is a fundamental operation in signal processing, with applications in radar, communications, and pattern recognition. Over the years, various optical architectures for one dimensional (1-D) correlation using acousto-optic devices (AODs) have been proposed and demonstrated [1-4]. The motivation for developing AOD-based correlation systems was in the real-time, wide instantaneous bandwidth nature of AODs that could give large (e.g., 10^6) time-bandwidth product real-time correlations of wide instantaneous bandwidth (e.g., 500 MHz) signals. In addition, 1-D AO correlators have also be used to perform 1-D signal spectrum analysis using the Chirp-Z algorithm [5-7].

Recently, we introduced an inherently stable in-line additive AO interferometer based on a cascaded design of two Bragg cells [3]. In this design, unlike the Mach-Zehnder interferometer, the Bragg cells also act as beam splitters and beam combiners in a compact, in-line design. We have shown that with the proper orientation of the Bragg cells, the optical system can be used to control phased array antennas [8-9]. In one system, the output of the optical system is a set of radio frequency or microwave signals with an appropriate signal phase distribution generated by electrically controlling the deflection angle of the two interfering beams [8]. In another system, the AO interferometer becomes the basis of stable rf/microwave frequency generation, with phased array antenna control provided optically using phase modulated nematic liquid crystal arrays [9]. It is also possible to use the AO in-line interferometer to form a wide instantaneous bandwidth space integrating optical spectrum analyzer that can be used as a microwave receiver [10]. In this system, the first Bragg cell in the cascade arrangement provides the broadband reference signal beam while the second Bragg cell is used for entering the input signal. A Fourier transform lens after the second Bragg cell simultaneously computes the spatial Fourier transform of the input signal and the broadband reference signal. At the output Fourier plane, the signal spectral components overlap/interfere with the appropriate reference spectral components, generating the desired immediate frequency (IF) signals.

This paper describes how the AO in-line interferometer can also be modified to implement the time integrated 1-D spectrum analysis and correlation functions. One feature of this architecture is that the correlation output does not have to be generated on a spatial carrier, thus saving the space-bandwidth product of the time integrating detector array, such as a CCD, for high resolution correlation detection. In addition, the use of the two AOD's in an interferometric design allows for linear phase and amplitude modulation of the signal and reference waveforms, without requiring bias level signals, as is required in a single AOD-based correlator design that uses an intensity modulated light source and an intensity modulated schliern imaged AOD. Thus, as a correlator, the proposed architecture optimizes the required minimum bias level in the output correlation signal, increasing the useful dynamic range of the detector. These, and other features of the architecture are discussed later in the paper.

Before we begin, another in-line AO correlator architecture will be experimentally demonstrated. This architecture was earlier demonstrated as a 1-D correlator [4]. We will further experimentally demonstrate it as a 1-D spectrum analyzer [3]. The limitations of this architecture, particularly, the fixed spatial carrier output, are highlighted, and solutions via the new in-line AO interferometer-based correlator are suggested.

0-8194-1275-9/93/$6.00

3. THE FIXED SPATIAL CARRIER AO CORRELATOR/SPECTRUM ANALYZER

Earlier, an in-line AO architecture shown in Fig.1 was proposed and demonstrated as a 1-D correlator and later as a spectrum analyzer [4,3]. The experiment in [3] is described as follows. The system consists of collimating optics, two counter propagating Bragg cells, imaging optics, and a time integrating detector. The light processing chain is as follows. The light from an He-Ne laser is collimated by an F=20 cm spherical lens. This collimated and expanded light is focussed by an F=30 cm cylindrical lens as a Bragg matched slit of light in a flint glass AOD. The AOD is driven by an external electrical signal $s_1(t)$. The +1 diffracted order and DC light, respectively, from the AOD are 1:1 imaged (with inversion) on to a second glass AOD (driven by an electrical signal $s_2(t)$), such that the +1 order light passes essentially unaffected through this second AOD, while the DC light is Bragg matched to produce a +1 order. A pair of F=20 cm spherical lenses are used in the 1:1 imaging system. The +1 orders from both AODs are imaged on to a CCD detector, after the DC light is blocked in the Fourier plane of the first imaging lens. The imaging is accomplished using F=20 cm and F=50 cm lenses, respectively, giving a magnification factor of 2.5. The optical field incident on the CCD is proportional to:

$$E(x,t) \propto \left[\tilde{s}_1\left(t-\frac{x}{Mv_a}\right)+\tilde{s}_2\left(t+\frac{x}{Mv_a}\right)\right] \text{ rect}\left(\frac{x - MX/2}{MX}\right) \qquad (1)$$

where v_a is the acoustic velocity in the Bragg cell, X is the AOD aperture, and M is the magnification of the imaging system. Here, $\tilde{s}(t)$ represents the analytic +1 order diffracted AOD drive signal. Depending on what the AOD drive signals are, this system can be used as a time integrating correlator or a 1-D spectrum analyzer, that uses carrier demodulation for bias removal. Different test experiments are carried out to demonstrate this ability. Using Eqn.1 , the intensity incident on the CCD can be written as:

$$I(x,t)=\left[\left|\tilde{s}_1\left(t-\frac{x}{Mv_a}\right)\right|^2+\left|\tilde{s}_2\left(t+\frac{x}{Mv_a}\right)\right|^2+2\,\text{Re}\left\{\tilde{s}_1\left(t-\frac{x}{Mv_a}\right)\,\tilde{s}_2^{*}\left(t+\frac{x}{Mv_a}\right)\right\}\right]\text{rect}\left(\frac{x - MX/2}{MX}\right) \qquad (2)$$

where the first and second terms are bias terms, while the third term gives the desired processor output. A spatial carrier modulated by the desired output can be observed across the CCD surface when the AODs are driven by their carrier signals, that is, $\tilde{s}_1(t)=\tilde{s}_2(t)=a\exp(-j\omega_0 t)$. In this case, the intensity detected on the CCD is given by :

$$I(x)=2|a|^2\left[1+\cos\left\{\frac{2\omega_0 x}{Mv_a}\right\}\right]\text{rect}\left(\frac{x - MX/2}{MX}\right) \qquad (3)$$

Here `a' is a constant amplitude term, and $\omega_0 = 2\pi f_0$ is the AOD center frequency. A 12 lines/mm spatial carrier is observed across the CCD that was obtained using a 57 MHz carrier frequency. One spatial cycle corresponds to approximately 4 CCD pixels. It is this spatial carrier that is used to modulate the desired signal, and later is electronically demodulated to remove any bias from the signal. The next step was to test the system to obtain autocorrelation of signals. First, the autocorrelation of linear frequency modulated (FM) signals is obtained. In this case, $\tilde{s}_1(t)=\tilde{s}_2(t)=a\exp[-j2\pi(f_0 t+0.5bt^2)]$, where `b' is the frequency sweep rate. The time integrated charge pattern on the CCD is given by:

$$Q(x)=\left[B_1+B_2\cos\left\{\frac{2\omega_0 x}{Mv_a}\right\}\text{sinc}\left\{\frac{2T_d b\, x}{Mv_a}\right\}\right]\text{rect}\left(\frac{x - MX/2}{MX}\right) \qquad (4)$$

where B_1 and B_2 are constants, and T_d is the CCD integration time. Thus, the autocorrelation of linear FM signals consists of a uniform bias level, and a spatial carrier modulated blur spot at the x=0 CCD position. The width of the blur spot is given by $\Delta x = Mv_a/T_d b$, and can be controlled by varying the sweep rate. Fig.2 shows the time integrated, carrier modulated blur spot video signal outputs for different sweep rates. Notice that the signal rides on a bias level that eats up part of the CCD dynamic range. The plot shown in Fig.3 records the behavior of the spot width as a function of FM sweep rate. This optical system using the linear FM signals can be used to perform signal spectrum

analysis if one of the FM signals is frequency or amplitude modulated by the test signal. In our experiment, we introduced the test signal s(t) as an amplitude modulated linear FM signal given by $s_2(t) = s(t)\cos[2\pi(f_0 t + 0.5bt^2)]$, where the single tone test signal of frequency f ' is $s(t) = a\cos(2\pi f' t)$. The resulting time integrated charge distribution on the CCD is given by:

$$Q(x) \approx \left[B_1 + 0.5B_2 \cos\left\{\frac{2\omega_0 x}{Mv_a}\right\}\left(\text{sinc}\left\{\frac{2T_d b x}{Mv_a} + f'\right\} + \text{sinc}\left\{\frac{2T_d b x}{Mv_a} - f'\right\}\right)\right] \text{rect}\left(\frac{x - MX/2}{MX}\right) \quad (5)$$

where we have assumed that f ' << f_0. This output corresponds to two carrier modulated blur spots positioned symmetrically around the x=0 position, where the position offset depends on the input signal test frequency f '. Thus, the frequency of the input signal has been mapped to a spatial coordinate space on the CCD sensor. Fig.4 shows the two carrier modulated spectral peaks riding on a bias level, while Fig.5 shows a frequency linearity plot of the processor. Note that the signal generators used for the FM and test signals, respectively, were free running and mutually incoherent. This resulted in a slow temporal oscillation of the time integrated spectral peaks over successive CCD integration frame times.

Next, for the sake of completeness, we also use this architecture to provide autocorrelation of AM signals, where in this case, $s_1(t) = s_2(t) = a\cos[2\pi f_1 t]\cos[2\pi f_0 t]$. Assuming that $1/T_d << f_1 << f_0$, the charge integrated by the CCD can be approximated as:

$$Q(x) \approx \left[B_3 + B_4 \cos\left\{\frac{2\pi\, 2f_1 x}{Mv_a}\right\}\cos\left\{\frac{2\pi\, 2f_0 x}{Mv_a}\right\}\right] \text{rect}\left(\frac{x - MX/2}{MX}\right) \quad (6)$$

where B_3 is the constant bias term, and B_4 is a constant factor. The expression in Eqn.6 consists of an amplitude modulated spatial carrier distribution. The read-out mechanism of the CCD converts this light pattern to a amplitude modulated video signal. The optical processor video signal outputs are shown in Fig.6.

The next section deals with a novel AO correlator architecture that does not have to generate the output signal on a spatial carrier, thus saving the useful space-bandwidth product of the CCD for the many spatially multiplexed parallel correlation channels. Moreover, this new design can be used with wide bandwidth Bragg cells, unlike the design in Fig.1, a point to be explained later; thus giving wideband signal processing capabilities.

4. THE NOVEL AO CORRELATOR/SPECTRUM ANALYZER ARCHITECTURE

The basic proposed optical architecture is shown in Fig.7 and is similar to the wide instantaneous bandwidth space integrating spectrum analyzer in ref. [10]. Note that the two imaging lenses between the Bragg cells cause the diffracted signal from the first Bragg cell to be spatially inverted when incident on the second Bragg cell. To form a time integrating correlator or spectrum analyzer, this signal beam spatial inversion has to be cancelled by using additional image inversion optics (such as a Dove prism) on the diffracted signal beam from the first Bragg cell, as shown by the image inversion optics box in Fig.7. This resulting optical modification in the AO interferometer generates two counter propagating spatial signals (the signal and reference) at the AOD2 plane that are imaged after AO diffraction on to a 1-D time integrating detector such as a 1-D CCD to generate the desired correlation/spectral peak. As shown in Fig.7, both the signal and reference beams are +1 order diffracted beams from AOD2 and AOD1, respectively. For spectrum analysis, the chirp-Z algorithm is used and the laser source is intensity modulated by the input signal c(t), with the Bragg cells fed by linear FM or chirp signals. Imaging optics is used after the second Bragg cell to send the diffracted light to a time integrating detector. In a similar fashion, the correlation of two signals r(t) and s(t) can occur with the same in-line AO interferometer if the two signals are fed to the two Bragg cells, as shown in Fig.7. In this case, the light source is not modulated.

The drive signals for the AODs can be expressed as $r(t) = s_1(t)\cos[2\pi f_0 t]$ and $s(t) = s_2(t)\cos[2\pi f_0 t]$, where $s_1(t)$ and $s_2(t)$ are real signals. The optical field incident on the CCD plane is the sum of two positive doppler shifted, counter-propagating, colinear beams, and can be written as:

$$E(x,t) \propto \left[s_1\left(t + \frac{x}{Mv_a}\right) + s_2\left(t - \frac{x}{Mv_a}\right)\right] \exp(-j2\pi f_0 t) \exp(j2\pi f_0 x/Mv_a) \quad \text{rect}\left(\frac{x - MX/2}{MX}\right) \quad (7)$$

The optical intensity can be expressed as:

$$I(x,t) = \left[\left|s_1\left(t + \frac{x}{Mv_a}\right)\right|^2 + \left|s_2\left(t - \frac{x}{Mv_a}\right)\right|^2 + 2\, s_1\left(t + \frac{x}{Mv_a}\right)\ s_2\left(t - \frac{x}{Mv_a}\right)\right] \text{rect}\left(\frac{x - MX/2}{MX}\right) \quad (8)$$

The first and second terms result in bias levels, while the third term gives the desired correlation output. Note that in this case, if the AODs are only driven by their carrier signals of amplitude ` a ', that is, $s_1(t)=s_2(t)=a$, then the time integrated intensity pattern at the output is a uniform light distribution, without a carrier (unlike the expression in Eqn.3), and is given by:

$$I(x) = 4|a|^2 \text{rect}\left(\frac{x - MX/2}{MX}\right) \quad (9)$$

For the case where the autocorrelation of AM signals is desired, and $s_1(t) = s_2(t) = a\cos[2\pi f_1 t]$, and assuming that $1/T_d << f_1 << f_0$, the charge integrated by the CCD can be approximated as:

$$Q(x) \approx \left[B_5 + B_6 \cos\left\{\frac{2\pi\ 2f_1\ x}{Mv_a}\right\} \right] \text{rect}\left(\frac{x - MX/2}{MX}\right) \quad (10)$$

where B_5 is a signal dependent bias level, and B_6 is a constant factor. An experiment is performed to demonstrate the working principles of the proposed architecture shown in Fig.7, and the results are shown to be consistent with the earlier analysis (Eqn.7-10). The laboratory architecture is shown in Fig.8. Here a Dove prism is used for the image inversion optics box shown in Fig.7. A 10 mW, 633 nm He-Ne laser beam is expanded, spatially filtered and collimated using a 10 X microscope objective, a 25 μm pin-hole, and a 20 cm focal length (FL) spherical lens S1, respectively. An iris is used to generate a 3.44 mm diameter beam that is incident at Bragg angle on the rf flint glass Bragg cell AOD1 that has a 10 μs time-aperture, a 12 mm acoustic beam height, a 70 MHz center frequency with a 40 MHz bandwidth, and a 3.9 mm/μs acoustic signal velocity. AOD1 is oriented so as to generate a +1 order positive doppler shifted diffracted beam. Both the diffracted and undiffracted (or DC order) beams from AOD1 are 1:1 imaged onto AOD2 (similar to AOD1) using the 25 cm FL spheres S2 and S3. AOD2 is oriented such that the DC light from AOD1 is used to generate a +1 order, positive doppler shifted diffracted beam which becomes colinear with the +1 order diffracted beam coming from AOD1. Note that in this arrangement, the acoustic signal propagation directions/vectors in both AODs are aligned, a condition required to generate a high quality correlation signal. Also note that this is not the case for the architecture in Fig.1.

Without the Dove prism shown inserted in the 1:1 imaging system between the two AODs, the acoustic signal propagation direction in AOD1 undergoes an image reversal when viewed in the AOD2 plane; this means that the diffracted signal spatial images from both AOD1 and AOD2 travel along the x-direction and are not counterpropagating, as required for generating a 1-D correlation operation. Thus, as shown in Fig.8, a Dove prism is placed in the path of the +1 order beam from AOD1, which cancels the image inversion caused by the 1:1 S2/S3 imaging system. It is well known that a Dove prism can be used for image inversion when illuminated by collimated light (see Fig.9). We have used this property in the experimental architecture, resulting in producing diffracted signal images from AOD1 and AOD2 that are counterpropagating in the AOD2 plane (AOD1 signal travels in the - x direction while the AOD2 diffracted signal travels in the x-direction). This pair of counterpropagating, positive doppler shifted, colinear, diffracted beams are 1 : M imaged onto a CCD time integrating detector array, M being the magnification of the S4/S5 sphere imaging system. The spheres S4 and S5 have FLs = 15 cm, making M = 1. A FL = 10 cm cylindrical lens C1 is added before the 2-D CCD to focus the light along the vertical or y-direction. The time integrating CCD detector generates the 1-D correlation along the x-direction of the CCD, where the correlation operation is calculated between the signal fed to AOD1 and the signal fed to AOD2.

5. EXPERIMENTAL RESULTS AND SYSTEM ISSUES

The carrier signal frequency chosen for driving the AODs is 100 MHz. At a 633 nm wavelength using the flint glass Bragg cells, this gives a relatively small angular beam separation of 0.93 degrees between the the +1 order and DC beams. The FL of sphere S2 is chosen to be long enough (FL= 25 cm) such that the +1 and DC beams from AOD1 are spatially separate, and a small Dove prism (dimensions, A = 6 mm, B = 8.5 mm, C = 25.37 mm; see Fig.9) can be carefully inserted in the +1 order beam, just before sphere S2. The prism input face has to be centered on the diffracted beam so that the beam emerges at the prism output face without any spatial deflection. In otherwords, the +1 order beam position remains unchanged with the insertion of the Dove prism, with the exception of the image rotation of the signal diffracted from AOD1. Note that for wideband Bragg cells that have much higher center frequencies (e.g., 3 GHz), the angular separation between the +1 and DC beams is much larger (e.g., 42.4 degrees), which leads to much shorter FL lens S2 being used to make the system, alongwith much easier placement of the Dove prism. When using wideband Bragg cells in the architecture in Fig.8, it is necessary to use some cylindrical optics to focus light into the very short acoustic height (e.g., 100 μm) of the wideband Bragg cells, and to recollimate the light before in enters the Dove prism. Note that use of wideband Bragg cells in the architecture in Fig.1 is a problem as the output spatial carriers can be exceedingly high (e.g., 1000 lines/mm), imposing a Nyquist sampling problem for the CCD, given the current pixel sizes (e.g., 20 μm).

The novel system in Fig.8 is tested as an autocorrelator for AM signals. A typical AM signal driving the AODs is shown in Fig.10. The AM signals have a 100 MHz carrier and a DC-10 MHz variable amplitude modulation. The signal in Fig.10 is generated by mixing a 100 MHz tone with a 5 MHz tone. The two signal generators are phase-locked. The AODs are driven by 4.66 volt-peak at 50 ohms AM rf signals that have been amplified by a 40 dB power amplifier. Fig.11 shows a series of results obtained from the optical processor. Oscilloscope traces showing a single video line from the CCD video camera and the corresponding image on the TV monitor are shown in Fig.11. The AM signal autocorrelations from the processor are the expected spatial frequency patterns that correspond to twice the AM modulation frequency (see Eqn.10), with a uniform signal dependent bias level. Because the two AODs are being fed by essentially equal amplitude signals, and the +1 diffracted beams from the two cells have similar optical power, the expected correlation modulation depth is close to a 100 %, as seen by the video line traces in Fig.11. Note that as the modulation frequency is increased, the frequency of the spatial carrier integrated by the CCD also increases. It is important to note that this system was built on an optical table where no air isolation was used and no special precautions were used to prevent air-based or other vibrations; nevertheless, the system which is based on the in-line AO interferometer provided the desired correlation outputs with processing times as large a 16.7 ms (1/60 seconds is one field time for video signals). The gaussian type apodization observed on the output correlation signals is due to the non-uniform gaussian illumination of the laser beam passing through an iris that was used to generate a narrow collimated beam.

Earlier in the paper, we have eluded to certain key features that the proposed architecture offers, particularly, when using wideband Bragg cells, when compared to other 2 AOD or 1 AOD/1-intensity modulated source based designs. The 2-AOD architecture, such as the one demonstrated in the earlier section (see Fig.1) cannot be used with wideband Bragg cells. This is because the Bragg angle at microwave frequencies is large and in order to get the desired diffracted orders in this architecture, the acoustic vector angle between the two Bragg cells is forced to be large (e.g., 42.5 degrees). This prevents the signals from the two AOD's to be aligned along one axis and counter-propagating, as required for the correlation operation. In addition, even for the low frequency rf cell case, the architecture in Fig.1 generates the correlation output on a relatively fast spatial carrier that eats up the valuable space-bandwidth product of the time integrating detector. This spatial carrier is proportional to the Bragg cell drive center frequency being used, and cannot be eliminated in this design. The proposed architecture (Fig.7) does not generate the output on a carrier, although, a carrier can be generated using an optical wedge on one of the beams between the two AODs, if required for bias filtering. Another way to generate the desired output correlation signal on a spatial carrier is by spatially offsetting the image inversion Dove prism that is placed in the Fourier plane between the two AODs (not before the first imaging lens between the AODs). In this case, a beam spatial translation in the Fourier plane results in a beam deflection at the CCD plane, thus generating an output correlation on a spatial carrier. When compared to the 1 AOD/1-modulated source-based correlators that use linear intensity modulation of a light source and the AOD, the architectures in Fig.1 and Fig.7 use linear amplitude/phase modulation of AODs in an interferometric design to generate the correlation output. Because high quality linear intensity modulation of Bragg cells and lasers requires a particular fixed and large bias level to be added to the signal waveform, less than optimum modulation depths are used for electrical-to-optical conversion in the system. This results in a much larger bias contribution versus the correlation signal contribution in the time integrated output of the optical correlator. These non-optimum (in terms of high signal modulation depth), high

bias levels driving the source and AOD eventually limit the correlator performance in terms of available or useful dynamic range, as the detector will eventually hit saturation. Another point to note is that the 1 AOD/single source-based correlators cannot be used as spectrum analyzers, unlike the designs in Fig.1 and Fig.7. Nevertheless, the proposed architecture in Fig.7 does have increased optical component and alignment complexity, suggesting a tradeoff in system complexity versus features.

6. CONCLUSION

We have experimentally demonstrated a spatial carrier-based AO in-line architecture for 1-D time integrating spectrum analysis. We have also introduced and experimentally demonstrated a novel AO architecture for 1-D signal correlation and spectrum analysis that is based on the stable AO in-line interferometer. This design does not require the correlation output to be generated on a spatial carrier. The architecture relies on image inversion optics, such as a Dove prism, although other variations of the basic architecture (Fig.7) are possible. The proposed system is experimentally demonstrated, generating the desired autocorrelation of AM signals. The proposed architecture is particularly suited for wideband Bragg cell implementation of wide bandwidth signal processing. Note that the architecture in Fig.7 can also be configured as a space integrating correlator, and will be described in later research.

7. REFERENCES:

[1] R. A. Sprague, `` A review of acousto-optic signal correlators,'' *Optical Engineering*, Vol.16, No.5, pp.467-474, Sept./Oct.,1977.

[2] W. T. Rhodes, `` Acousto-optic signal processing: convolution and correlation,'' *Proc. of the IEEE*, Vol.69, No.1, pp.65-78, Jan., 1981.

[3] N. A. Riza, `` Novel acousto-optic systems for spectrum analysis and phased array radar signal processing," Chapter 5, pp.160-186, Ph.D dissertation, (California Institute of Technology, Pasadena, Calif., 1989) in *University Micofilms*, Ann Arbor, MI.

[4] D. Psaltis, J. Yu, and J. Hong, `` Bias-free time integrating optical correlator using a photorefractive crystal,'' *Applied Optics*, Vol.24, No.22, Nov., 1985.

[5] R. M. Montgomery, ``Acousto-optical signal processing system,'' U.S. Patent 3,634,749, Jan., 1972.

[6] R. A. Sprague and C. L. Koliopoulos, `` Time integrating acoustooptic correlator, '' *Applied Optics*, Vol.15, No.1, Jan., 1976.

[7] T. M. Turpin, `` Spectrum Analysis using optical processing, '' *Proc. of the IEEE*, Vol.69, No.1, pp. 79-92, Jan., 1981.

[8] N. A. Riza and D. Psaltis, ``Acousto-optic signal processors for transmission and reception of phased array antenna signals," *Applied Optics*, vol.30, no.23, pp.3294-3303, 1991.

[9] N. A. Riza, `` A compact high performance optical control system for phased array radars,'' *IEEE Photonic Technology Letters*, Vol.4, pp1072-1075, 1992.

[10] N. A. Riza, ``Optically efficient interferometric acousto-optic architecture for spectrum analysis," *Applied Optics*, Vol.31, No.17, pp.3194-3196, June 10, 1992.

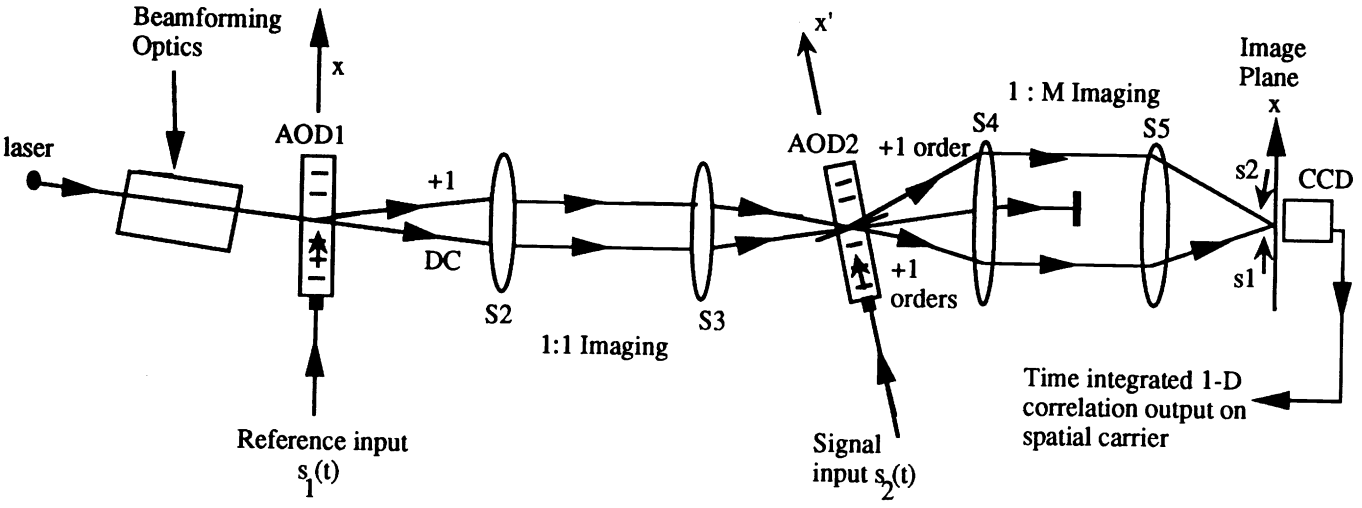

Note: Angle between acoustic directors x and x' is twice the Bragg Angle; Ideally it should be zero.

Fig.1 The fixed spatial carrier in-line AO architecture for 1-D correlation and spectrum analysis.

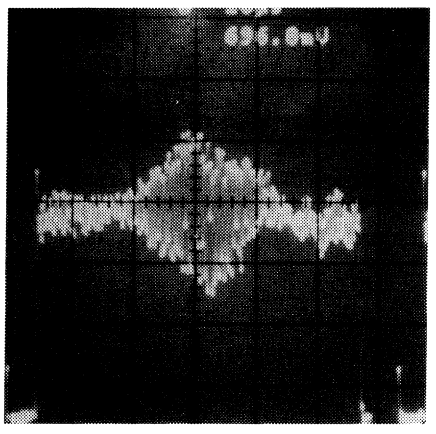

(a)

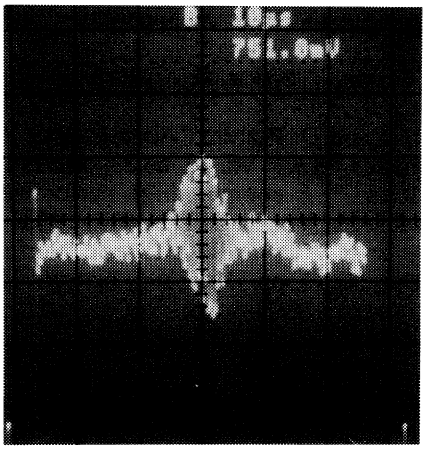

(b)

Fig.2 Time integrated, carrier modulated, autocorrelation outputs (blur spots) for different sweep rate FM signals. (a) 63 MHz/s, (b) 138 MHz/s.

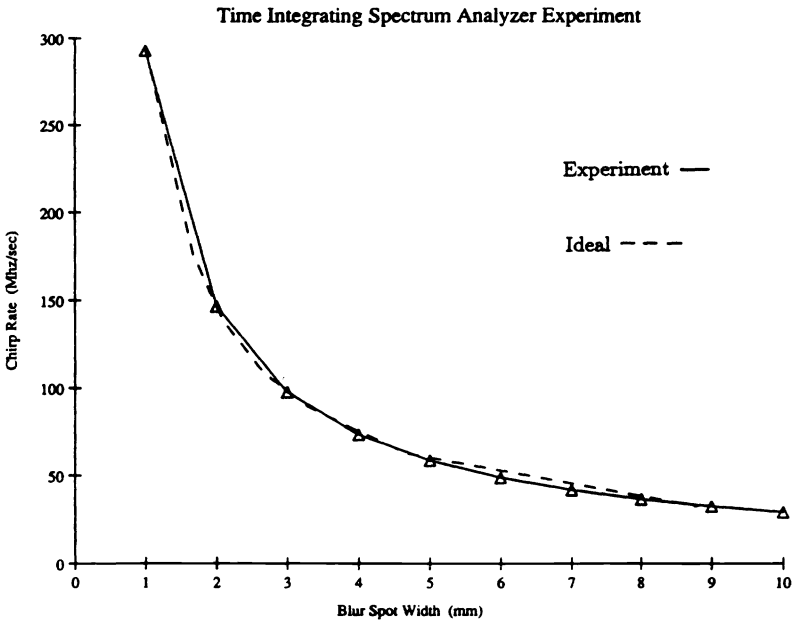

Fig.3 Plot of autocorrelation blur spot width versus sweep rate of linear FM signals.

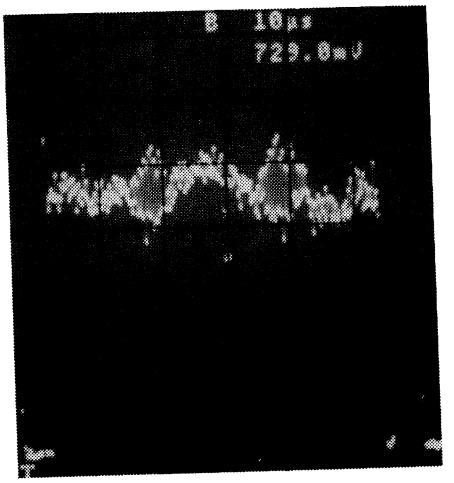

Fig.4 Double sided, carrier modulated spectral peaks from the time integrating spectrum analyzer for a 140 Hz AM signal input.

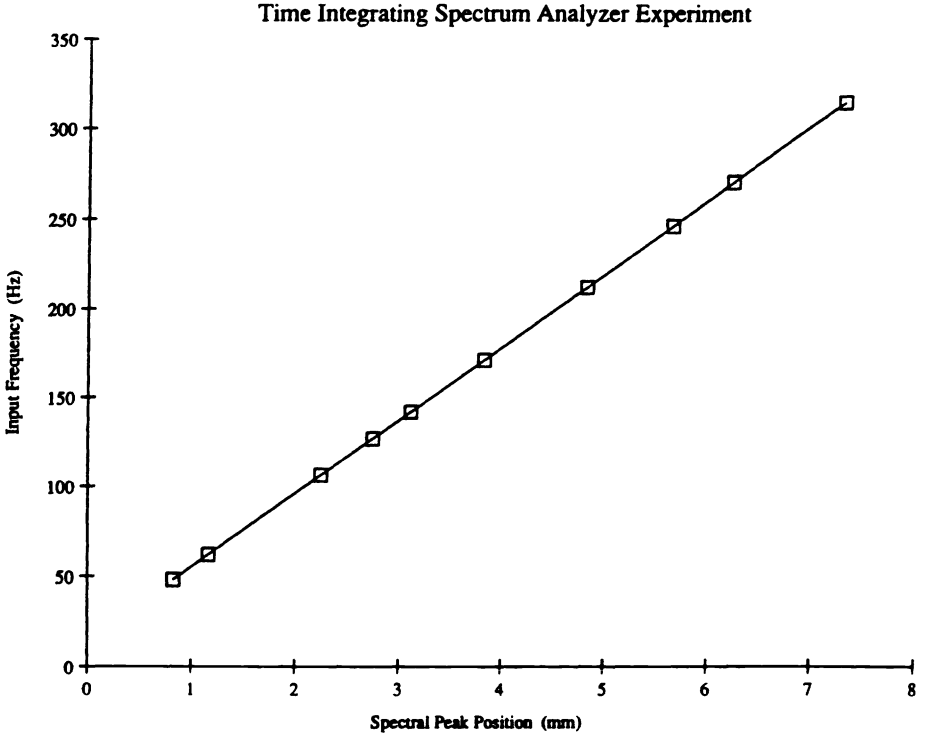

Fig.5 Plot of frequency linearity of the experimental spectrum analyzer.

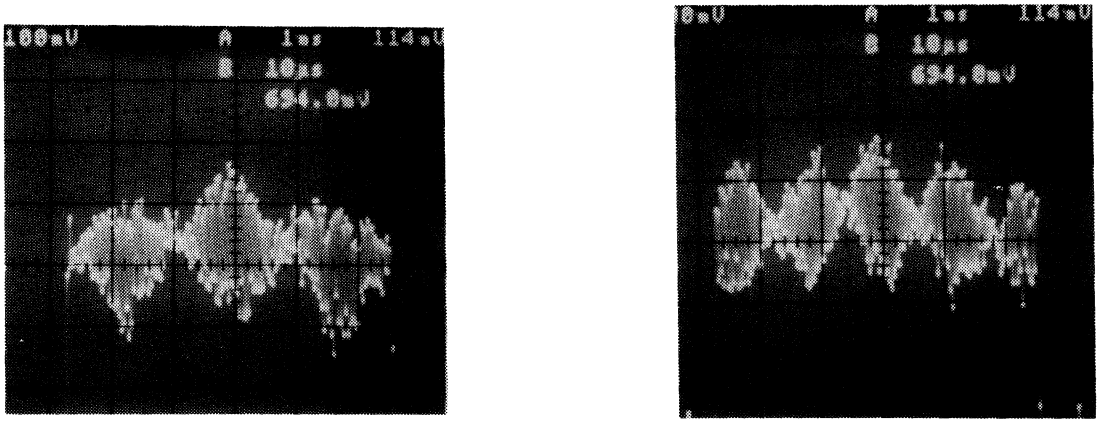

(a) (b)

Fig.6 Carrier modulated AM signal autocorrelation outputs from the optical processor for different AM inputs on a 57 MHz carrier. (a) 1 MHz AM, (b) 1.35 MHz AM.

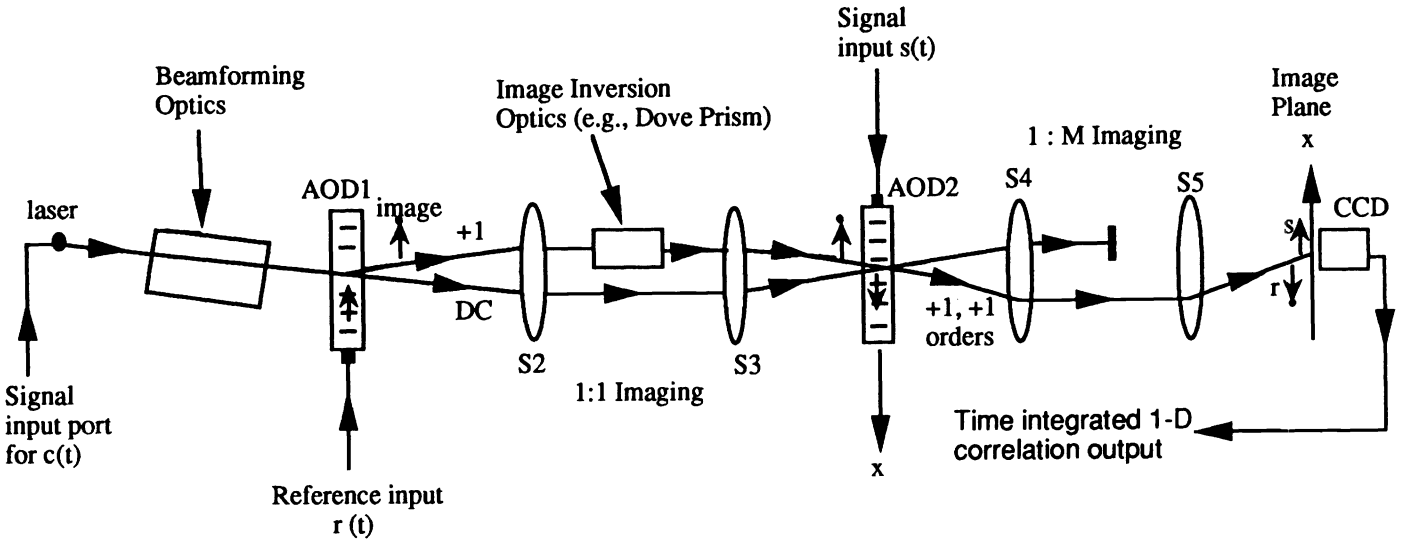

Fig.7 The basic proposed optical architecture of a 1-D time integrating correlator/spectrum analyzer using the in-line AO interferometer.

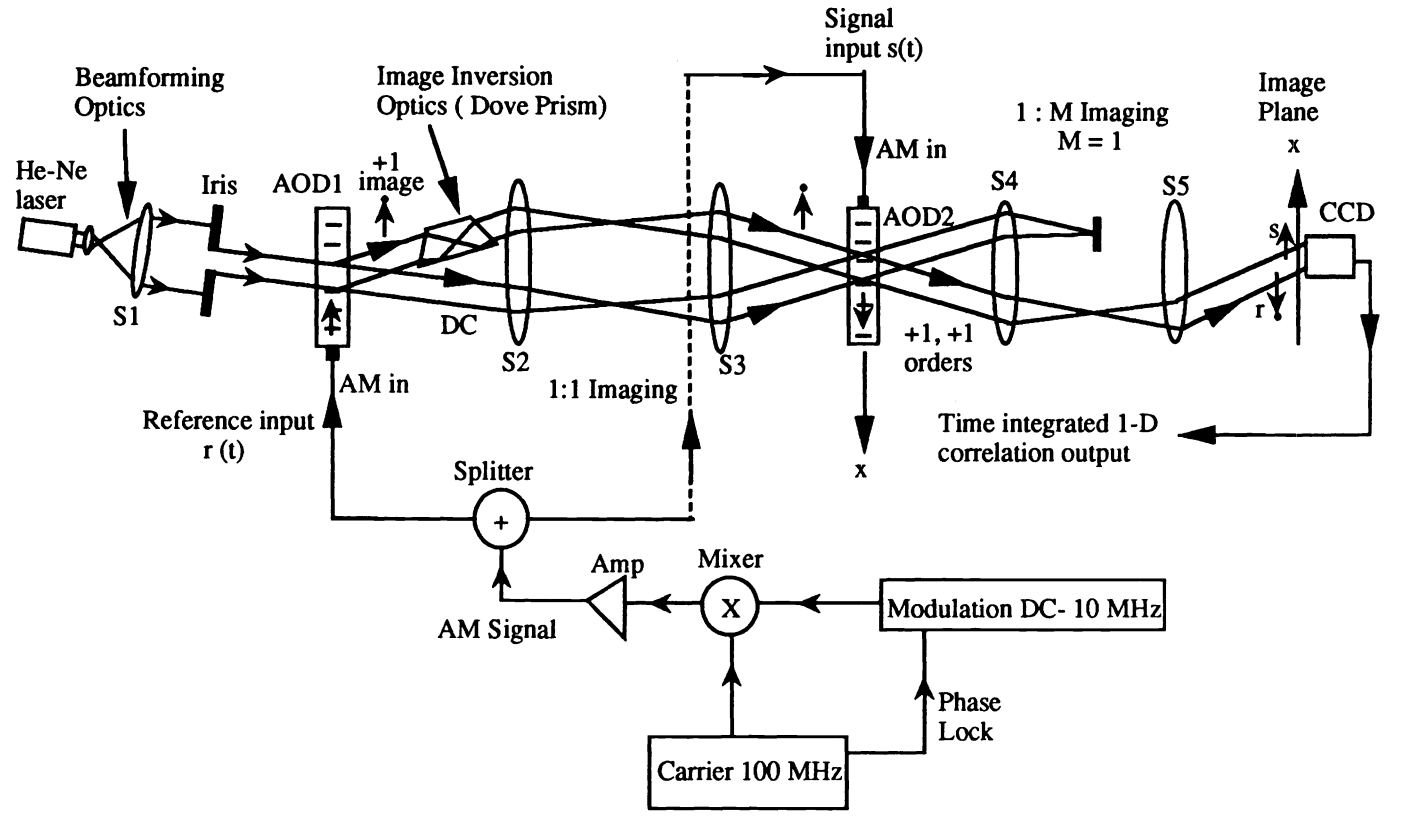

Fig.8. System diagram of a version of the proposed correlator/spectrum analyzer architecture that is implemented in the laboratory.

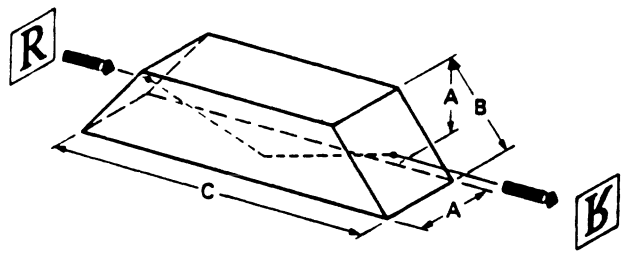

Fig.9. Optical image inversion using a Dove prism (Melles Griot Catalog).

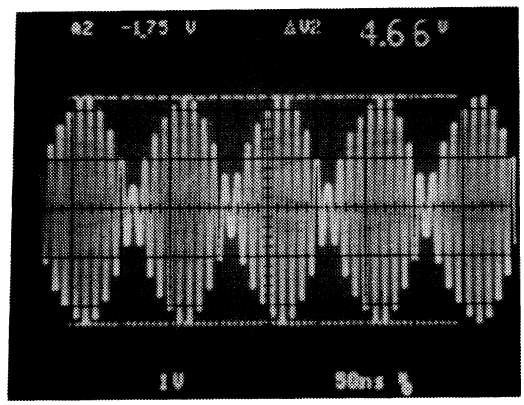

Fig.10. Oscilloscope trace of a typical AM signal used as input to the system. Here, the carrier is 100 MHz with a modulation of 5 MHz.

(a)

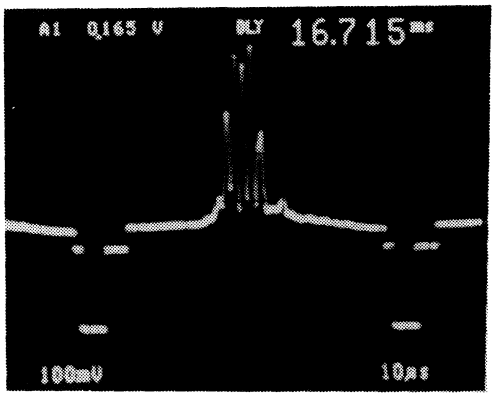

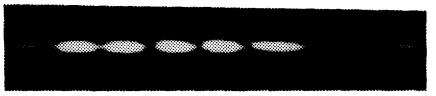

(b)

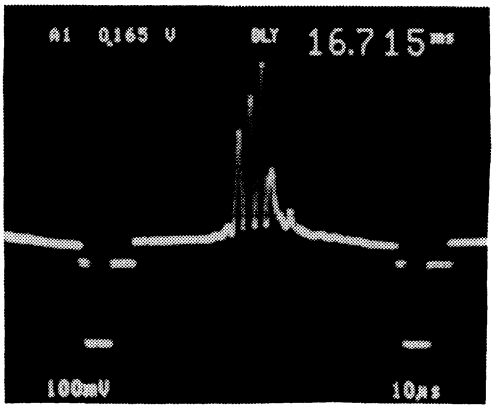

(c)

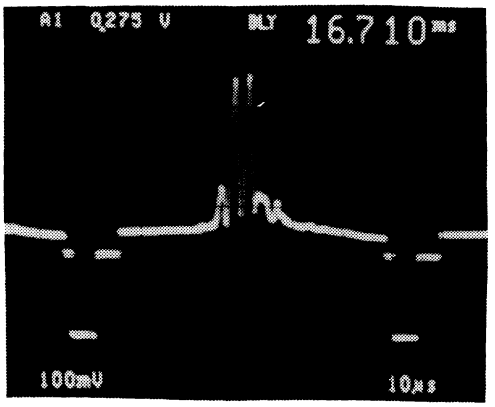

Fig.11 A series of autocorrelation results obtained from the optical processor as the modulation frequency is varied: (a) 7 MHz, (b) 5 MHz, and (c) 4 MHz. The photographs show the CCD video line trace and the corresponding image seen on the monitor.